Processing and Application of Ceramics 15 [1] (2021) 1–10
https://doi.org/10.2298/PAC2101001M

Kinetic evaluation of YSZ/Al_2O_3 nanocomposite coatings fabricated by electrophoretic deposition on a nickel-based superalloy

Leyla Mostafapour[1], Saeid Baghshahi[1], Masoud Rajabi[1], Seyed Mahdi Siahpoosh[2,*], Fateme Esfehani[1]

[1]*Department of Materials Science & Engineering, Faculty of Technology and Engineering, Imam Khomeini International University (IKIU), Qazvin, Iran*
[2]*Department of Materials & Metallurgy Engineering, College of Technology and Engineering, Takestan Branch, Islamic Azad University, Takestan, Iran*

Received 23 March 2020; Received in revised form 14 October 2020; Accepted 14 December 2020

Abstract

In the current study, the evolution of deposition yields with time for yttria stabilized zirconia (YSZ)/Al_2O_3 nanocomposite coatings deposited by electrophoretic technique was described by a kinetic model. Aluminium powder was used as a sintering aid and also the source for the formation of Al_2O_3 during sintering. A mixture of ethanol and acetylacetone was utilized as the solvent. In order to prepare a stable suspension, surface charges and electrostatic interaction between particles in suspensions were evaluated through analyses of pH, zeta potential, and particles size. Electrophoretic deposition (EPD) on Inconel 718 electrodes was successfully carried out by employing three well-dispersed suspensions including nanostructured YSZ with 0, 30 and 50 wt.% of Al particles. The influences of three different applied voltages (25, 45 and 65 V), deposition time and the weight percent of Al particles on the EPD kinetic at a time interval of 0–300 s were studied and quantified based on the Baldisserri equation. It was shown that the results achieved from the Baldisserri model were almost well matched with the experimental data within a wide range of time. It was found that the deposition rate declines with the increase in YSZ nanoparticles content and time. The coated substrates in the final step were dried and sintered at 1150 °C. The coating quality and surface morphology were characterized by field emission scanning electron microscopy (FE-SEM).

Keywords: *YSZ/Al_2O_3 coatings, electrophoretic deposition, kinetic modelling, deposition yields*

I. Introduction

The preparation of Y_2O_3 stabilized ZrO_2 (YSZ) deposits has attracted increasing attention from the scientific communities over the past few decades, because of their excellent toughness, high mechanical and erosion resistance, high melting point, low thermal conductivity, relatively high coefficient of thermal expansion and good ionic conductivity [1], as well as their potential for use in solid state electrochemical devices such as fuel cells [2,3], gas sensors [4–6] and also thermal barrier coatings [7,8].

The thermal barrier coatings (TBCs) are mainly from the group of zirconia ceramics which can create protective layer on the metal substrate. The most outstanding role of TBCs is to insulate heat transfer and to decrease the temperature of the underlying metallic substrates. Because of that, they can play an important role in protecting parts used at high operating temperatures, such as gas turbines, while maintaining thermo-mechanical and chemical stability [9,10]. Yttria stabilized zirconia (YSZ) [11] and alumina (Al_2O_3) [12,13] coatings are currently considered as TBCs.

Several routes such as thermal plasma spray (TPS) [14,15], electron beam physical vapour deposition (EB-PVD) [9], chemical vapour deposition [16] and electrophoretic deposition (EPD) [11] have been employed to produce TBCs. Among the available deposition techniques, EPD is a potential processing technique for the fabrication of high-performance and high-perfection ceramics and coatings and small parts with complicated

*Corresponding author: tel: +98 9122815694,
e-mail: *sm.siahposh@gmail.com*

shapes [17]. This method can yield a number of advantages over the usual coating approaches, including short formation time, low expense, simplicity in instrumentation, production versatility for coating on non-planar substrates such as complex-shaped implants, and capability for mass production [2,18]. Besides, it has been found that nanostructured coatings fabricated by EPD process have high chemical uniformity, decreased flaw size and microstructural homogeneity, and require a lower sintering temperature for densification [18–20].

Compared with other common methods for making TBCs, electrophoretic deposition has been widely considered because it is easy to control the process execution and flexibility in microstructural manipulation. However, it is now well known that the control of thickness, density, homogeneity and quality of final coating not only depends on the deposition time, solvent and dispersant type, particle size and morphology, but also significantly depends on the EPD mechanisms and the effects of applied potential [21,22]. Nevertheless, there is a lack of an adequate understanding of the mechanisms up to now. One important approach to the understanding of the mechanisms of EPD has been to study the kinetic behaviour of suspended particles in the media or time dependence of deposited mass [23,24].

Recently, Collini *et al.* [25] have described the kinetics of deposition of titanium carbide films from aqueous and propylene carbonate-based suspensions by the well-established Sarkar model of EPD [22]. However, this model is only valid if the suspension and deposit resistances are comparable, while a correction is needed when the deposit resistance is remarkably higher than that of the suspension, as usually happens due to the passivisation and shielding effect of growing insulating layer [25,26]. Verma *et al.* [27] proposed a new simulation tool based on the finite difference method (FDM) for modelling of electrophoretic deposition of paint films. Baldisserri *et al.* [28] developed a mathematical relationship between some characteristics of TiO_2 deposits (such as thickness, density and resistivity) and the electrical current transients in EPD process for ethanol-based colloidal suspension as the solvent. It has been shown that the Baldisserri model is capable to predict precisely the rate of layer formation for EPD process of hydroxyapatite-titania nanocomposite, and thus it can well reproduce the experimental data when compared to other semi-empirical kinetic equations [29]. However, as far as we know, there have been no research efforts devoted to examining this approach for description of deposition kinetics of TBCs. Herein, for the first time, the obtained experimental results and kinetics of electrophoretic deposition from YSZ/Al suspensions with 0, 30, and 50 wt.% aluminium were explained with the Baldisserri model. The combination of high hardness and Young's modulus of the Al_2O_3 with the additional toughening effect provided by the ZrO_2, has been reported to lead to an increase in the flexural strength and fracture toughness of coatings.

Inconel 718 is a high strength metal and one of the nickel-based superalloys which are extensively utilized in the aerospace industry for the hot sections of gas turbine engines [30]. Therefore, its coating is of great importance for such applications. Thus, the main aim of the current work is to evaluate the validity of the Baldisserri model for the kinetic description of deposition of YSZ/Al_2O_3 nanocomposite onto Inconel 718 by electrophoretic technique. The changes related to the constants of the Baldisserri model and the degree of matching of the experimental data with this model were verified and quantified for different suspensions under various voltages.

II. Experimental

2.1. Materials

The starting materials used in this study were zirconia nanopowder stabilized with 3 mol% yttria (3%YSZ, >99%, Jiaozuo Huasu Chemical Co., Ltd., China) as the coating material, aluminium powder (>99.5%, PMC, Iran) as the source for aluminium oxide formation and a sintering aid, iron (III) oxide (Fe_2O_3, >99.5%, Alfa Aesar, UK) as another sintering aid and iodine (Merck, Germany) as adjuster of the particles surface charge in suspensions or dispersant. A mixture of ethanol (>99%, Sigma-Aldrich, UK) and acetyl-acetone (ACAC, >99%, Sigma-Aldrich, UK) with a volume ratio of 1:1 was used as the solvent.

2.2. Process of EPD

In the first step, 20 ml of acetylacetone and ethanol mixture solvents with a volume ratio of 1:1 were prepared. Thereafter YSZ nanoparticles, aluminium powder, iodine and iron oxide were added to the solvents mixture to produce suspensions with YSZ/Al total concentration of 20 g/l. Three suspensions with different amounts of YSZ and Al (YSZ, YSZ-30 wt.% Al and YSZ-50 wt.% Al) were prepared. The detailed description of the preparation conditions for different suspensions is summarized in Table 1. In order to prevent agglomeration, the resulting suspension was then agitated on a magnetic stirrer apparatus for 45 min. Afterwards, it was placed for 15 min in an ultrasonic bath (35 kHz).

The EPD cells contained two Inconel and stainless steel electrodes with a distance of 10 mm. Electrodes were submerged parallel to each other in suspension. Stainless steel was used as the anode material, whereas the cathode electrode was made of Inconel 718 sheets having 2.5 mm thickness. The steel and Inconel 718

Table 1. The amounts of starting materials utilized for the preparation of different suspensions

Suspension	YSZ [g/l]	Al [g/l]	I_2 [g/l]	Fe_2O_3 [g/l]
YSZ-50 wt.% Al	10	10	0.5	0.16
YSZ-30 wt.% Al	14	6	0.5	0.16
YSZ	20	0	0.5	0.16

were cut precisely into rectangular-shaped substrates with dimensions of $10 \times 10\,mm^2$. Prior to coating, the metallic substrates were washed with detergent and distilled water and then degreased with acetone and then dried in the air at the room temperature. Electrodes were connected to DC power supply to provide the driving force needed for the layer formation. The process of deposition was performed by varying the voltage and suspension composition, while the values of all other EPD parameters were taken as constant.

After drying, the coated substrates were subjected to a two-step sintering procedure in an electrical furnace. In the first step, the sample was heated in air atmosphere up to the temperature of 650 °C with the rate of 2 °C/min and kept for 5 h at this temperature, where aluminium melting starts to take place [31]. The initiated Al melting increases connections between particles and refines bonding strength, which in turn leads to suppressing the cracks propagation in the coating. This event is followed by the oxidation of aluminium and subsequent formation of Al_2O_3 as secondary phase [32]. In the second step, the sample having now Al_2O_3 phase was heated to 1150 °C with the same rate and kept for 4 h at this temperature to increase the adhesion and the density of the coating. Finally, it was allowed to cool down to ambient temperature in the furnace.

2.3. The methodology of the kinetics study

In order to evaluate the kinetics of layer formation, the coating weights obtained from different prepared suspensions under three applied voltages (25, 45 and 65 V) were measured. For this purpose, the cross section area of the electrodes, the total concentration of the powders in suspension and the stabilizer amount was considered constant, and parameters of the time and voltage were changed. Then by applying different voltage values, the process of the coating was performed with three different suspension compositions. After drying the samples for 24 h, the weight difference of the samples before and after the layer formation was considered as coating weight and these results were used to study the kinetics of the layer formation.

During preparation of the coating, the relationship between current density variations with time was recorded for 300 s. These data were measured at specified moments by the corresponding range amperemeter connected in series with the system. Plots were analysed by data fit software. In order to correlate with the Baldisserri formula, at first, the current density-time trends were plotted. Then plots of passed charge versus time were derived from time integrals of the current transients. Then, by plotting weight of coating W relative to the passed charge q, constant k (mass to passed charge ratio) corresponding to the Baldisserri formulation was obtained:

$$W(t) = k \cdot g(t) \tag{1}$$

For each voltage, the value of $2A \cdot k \cdot j_0$ expression was calculated separately and incorporated in the following formula to determine constant α:

$$W(t) = \frac{2A \cdot k \cdot j_0}{\alpha}\left(\sqrt{1 + \alpha \cdot t} - 1\right) \tag{2}$$

where A is the area of the working electrode, j_0 is the initial current density, and V is the deposition voltage. ρ_D and d_D are the resistivity and density of deposit, respectively, and α is:

$$\alpha = \frac{2j_0^2 \cdot k}{V}\left(\frac{\rho_D}{d_D}\right) \tag{3}$$

2.4. Characterization

In order to evaluate the surface quality of sintered coatings, the field emission scanning electron microscopy (FE-SEM) images were captured on a Mira3 Tescan (Brno, Czech Republic) by a back-scattered electron detector. The coated sample was cut by Wire Cut Electrical Discharge Machining to examine the microstructural characteristics of cross-section surfaces by using the secondary electron images of FE-SEM.

Zeta potential and particles size of the suspensions were measured by means of Zeta seizer HS 3000 electrophoretic light scattering instrument (Malvern Ltd, UK). The pH changes in the suspension due to dispersant addition were continuously monitored by utilizing a pH meter.

III. Results and discussion

Figure 1a shows the XRD pattern and TEM micrograph of the used YSZ nanopowder provided by the manufacturer. It can be seen that the powder contains tetragonal phase as well as a slight amount of monoclinic phase, and its mean particles size is about 50 nm. The particles sizes of the used aluminium powder in the as-received form were less than 60 μm. The XRD pattern for this powder is shown in Fig. 1b.

3.1. Analysis of surface charges in suspension

Aqueous and non-aqueous (organic) solvents can be used to prepare suspensions. Herein, suspensions with organic solvents were considered due to low dielectric constant and no degradation during applying of the voltage. The disadvantage of using non-aqueous medium is that the particles are more difficult to stabilize [33]. Therefore, the suspensions were prepared by adding iodine as suspension stabilization agent to help disperse powders and reduce flocculation. In this section, the effect of iodine as a stabilizing agent on the surface charge was investigated.

The changes of the zeta potential of EPD solution, the average size distribution of the particles and pH values are plotted as functions of the amount of iodine added to the solution in Fig. 2. As it is seen in Fig. 2a, in absence of iodine, the suspension exhibits a low zeta potential value of about 9.6 mV. As iodine concentration increases from 0 to 0.5 g/l, zeta potential of the sus-

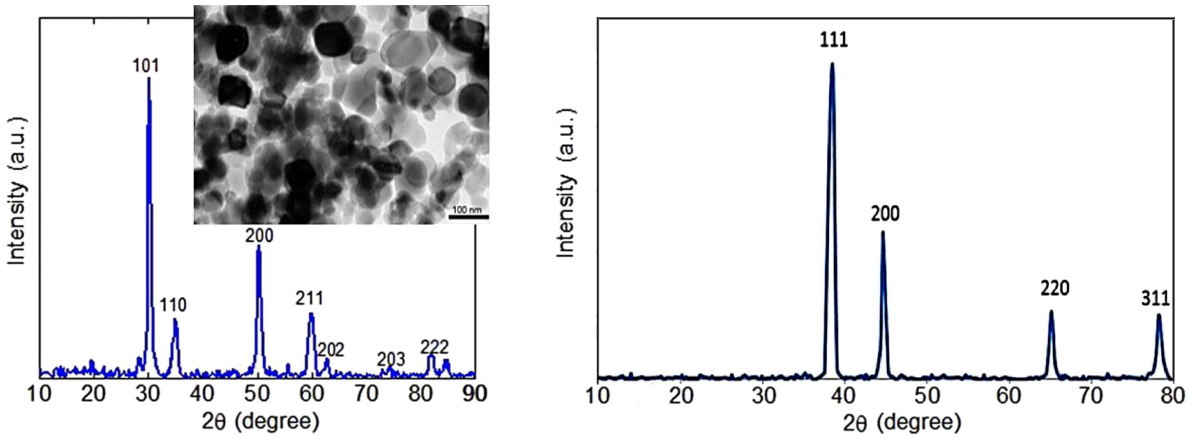

Figure 1. XRD pattern and TEM image of yttria-stabilized zirconia powder (a) and XRD pattern of aluminium powder (b)

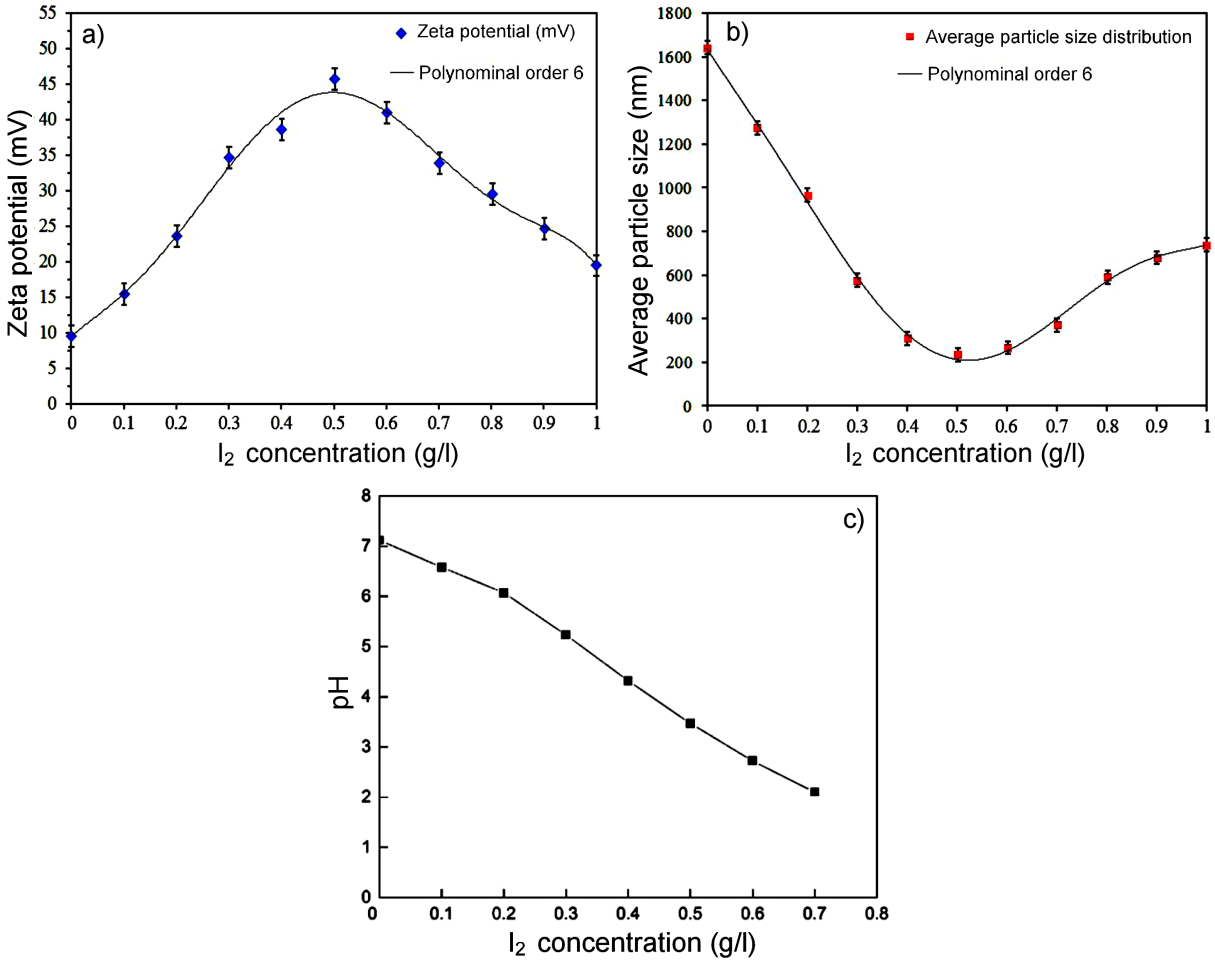

Figure 2. The values of zeta potential (a), average size distribution of particles (b) and pH (c) as functions of iodine added to the suspensions containing the mixture of ethanol-acetylacetone with 1:1 volume ratio

pension increases up to the maximum value of 45.7 mV. From Fig. 2b, it can also be observed that during the procedure of iodine addition up to 0.5 g/l, the average particle size distribution is simultaneously reduced to the minimum of 232.5 nm, which is noticed to be the optimum point. The initial increase in zeta potential with iodine addition can be attributed to the adsorption of formed H^+ ions onto the particles surface. These positive ions are generated by the following proposed reactions between I_2 and acetylacetone as well as I_2 and ethanol [31,34,35]:

$$CH_3{-}CO{-}CH_2{-}CO{-}CH_3 + 2\,I_2 \leftrightarrow I{-}CH_2{-}CO{-}CH_2{-}CO{-}CH_2{-}I + 2\,H^+ + 2\,I^- \quad (4)$$

$$CH_3{-}CH_2{-}OH + I_2 \leftrightarrow I{-}CH_2{-}CH_2{-}OH + H^+ + I^- \quad (5)$$

As noted in reactions 4 and 5, the addition of iodine to the suspension causes the release of H^+ and I^- ions and a number of protons surrounds the particles and can cause particles surfaces to become charged. H^+ concentration seems to increase with an increment in the amount of iodine, and becomes excessive when iodine concentration exceeds 0.5 g/l. By increasing H^+ above its optimum value, the surface charge of particles saturates and the free positive ions that are formed carry some electrical charge, and the corresponding zeta potential declines. Therefore, interparticle electrostatic repulsive force decreases when iodine concentration is increased beyond 0.5 g/l. Consequently, the colloidal stability is reduced and agglomeration of particles is induced [36,37]. The colloidal stability of the particles has a great influence on the deposition rate and the final microstructure of the coatings. So the quality of the final coatings was confirmed to be affected by it [37,38]. Similar results with respect to the zeta potential decrease at higher dispersant concentration have been reported by Das *et al.* [39] and Ishihara *et al.* [34] for preparation of YSZ thin films by using phosphate ester and iodine as the dispersant, respectively. Hence, suspension with an iodine concentration of 0.5 g/l was utilized throughout this investigation.

As it can be observed from Fig. 2c, the pH of the solutions with iodine content shows a descending trend, indicating an enhancement in the H^+ ion concentration. This finding is consistent with the result of pH reduction via iodine addition, achieved by Santillán *et al.* [40], for acetylacetone suspension containing 1 wt.% TiO_2.

3.2. Kinetic analysis

Kinetic models can play a key role in better understanding of the layer formation rate by EPD process. Figure 3 displays variations in the current density over deposition time (during 300 s) recorded at three different constant potentials of 25, 45 and 65 V applied to the YSZ, YSZ-30 wt.% Al and YSZ-50 wt.% Al suspensions. As it can be seen, in the initial stages of the layer formation, current density decreases rapidly and then approaches a constant value after a given time, which has been attributed to the electrode polarization and/or formation of a deposited insulating layer [41,42]. However, the slope of the curves in Fig. 3 increased with increasing the voltage and the amount of YSZ nanoparticles, which can be ascribed to more influence of the formation of an insulating layer of ceramic particles on the electrode surface as deposition continues [27].

The amount of passed electrical charge under different experimental conditions was calculated by time integrals of the current density curves, as represented in Fig. 4. At all voltages, charge variations relative to the time dQ/dt have declined over deposition time, and due to the formation of a ceramic insulating layer, the dQ/dt (slope) becomes constant at longer times. Also, an increase in the voltage enhances the mobility of the suspended particles and increases the amount of passed electrical charge.

However, the lower difference between passed charges at 45 and 65 V than between those at 25 and 45 V can be explained by the gradual change in EPD mechanisms from the deposition controlling mode to the diffusion controlling mode [29]. In the diffusion controlled mechanism, the gradual decrement in electrical conductivity of the deposit by increasing deposit thickness results in a sharp drop in electrical field intensity at the outer deposit layer and consequently, the driving force for the continuation of layer formation decreases. In the deposition rate-controlling mechanism, van der Waals and steric forces overcome the electrostatic repulsion forces between particles, and the pressure exerted on initially deposited particles by those deposited later leads to the particles compressing [23].

Figure 5 illustrates linear changes of the deposit weight as a function of passed charge. In each coating composition, as the charge increases, the deposit weight is also increased. The maximum slope k indicates the higher mobility of the particles in the suspension, which originates from increased electrical charge, and ultimately leads to an enhancement in the deposition yields.

The results of the Baldisserri model were also superimposed on Fig. 5 to generally describe different plots. The ability of the used equation in the precise prediction of deposit weight was quantitatively evaluated by

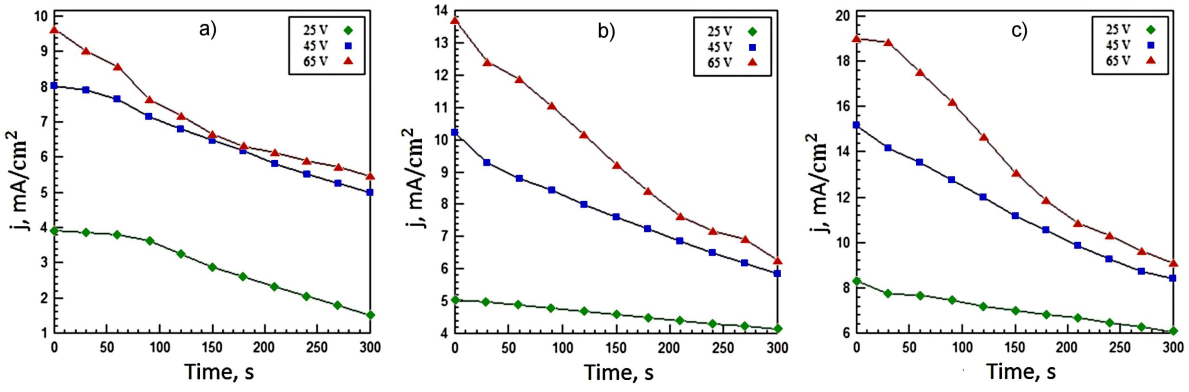

Figure 3. The influence of various voltages on changes in current density with time for different suspensions: a) YSZ-50 wt.% Al, b) YSZ-30 wt.% Al and c) YSZ

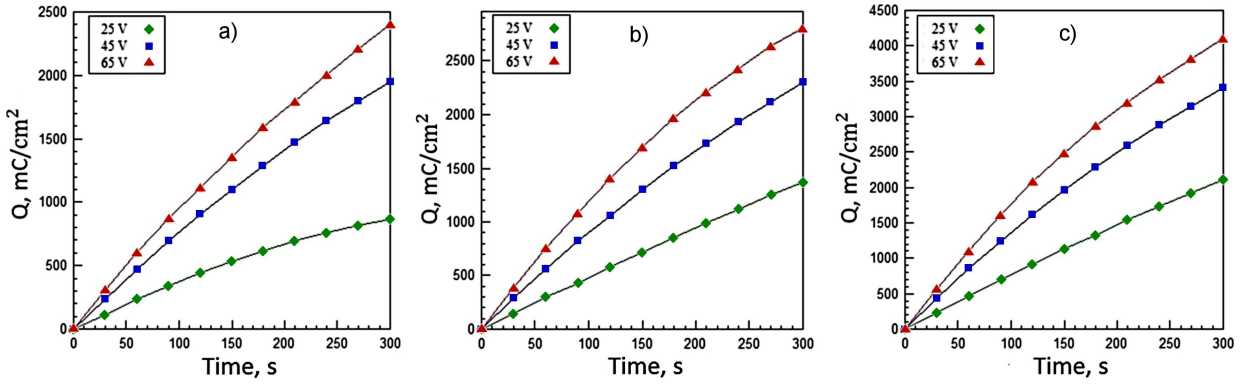

Figure 4. Effect of different voltages on calculated passed charge with time for different suspensions: a) YSZ-50 wt.% Al, b) YSZ-30 wt.% Al and c) YSZ

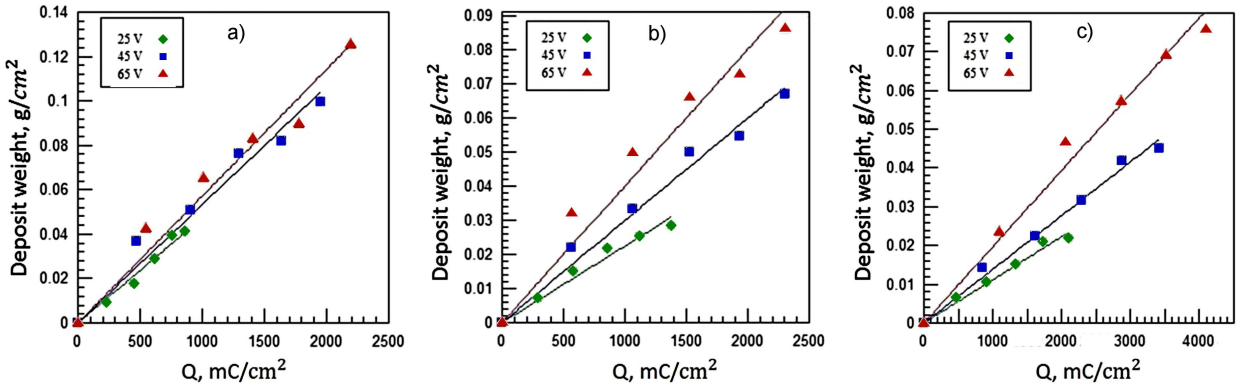

Figure 5. Effect of different voltages on coating weight variations against the passed charge as well as a general description of different curves by using linear relationships for different suspensions: a) YSZ-50 wt.% Al, b) YSZ-30 wt.% Al and c) YSZ

employing R^2 value as the correlation coefficient factor [43]. Along with experimental measurements, the set of regression constants calculated from data fitting is given in Table 2. As it can be seen, values of R^2 indicate that relatively good matching between experimental data and the Baldisserri model predictions is achieved, which can be ascribed to the consideration of both the insulating effect of growing layer and the concentration change of suspended particles, featured by this approach.

Based on the results given in Table 2 it can be concluded that by increasing voltage in each constant suspension composition for the process of layer formation, the coefficient k, as well as the constant α of the kinetic model, increased. Considering a constant voltage, with an increase in the percentage of aluminium in suspension, the k value increased, which indicates that the Al particles tend to be more precipitated on the electrode.

Furthermore, the results of initial current density at different conditions are summarized in Table 2. It is observed that as the amount of YSZ nanoparticles increases, the initial current density also increases. This fact can be attributed to the electrical conductivity of suspension, because there is an optimum range of conductivity to produce good deposition yields [44]. By increasing the level of electrical conductivity of the suspension to an excessive value, a large number of free ions are generated in the suspension [45]. This

Table 2. The calculated constants of the Baldisserri model based on the obtained experimental data

Deposit composition	Voltage	α [10^{-3}/s]	k [10^{-5}g/C]	j_0 [mA/cm^2]	$2A \cdot k \cdot j_0$ [mA/cm^2]	R^2	Conductivity [μS/cm]
YSZ	25	3.66	1.11	8.30	18.43	0.98	118
	45	5.64	1.36	15.16	41.24	0.97	
	65	6.95	1.97	19.00	74.86	0.96	
YSZ-30 wt.% Al	25	1.74	2.24	5.02	22.49	0.97	96
	45	6.12	2.99	10.22	61.12	0.97	
	65	20.70	4.00	13.70	109.6	0.98	
YSZ-50 wt.% Al	25	3.93	4.73	3.90	36.89	0.98	85
	45	4.83	5.33	8.02	85.49	0.94	
	65	6.32	5.72	9.64	110.28	0.95	

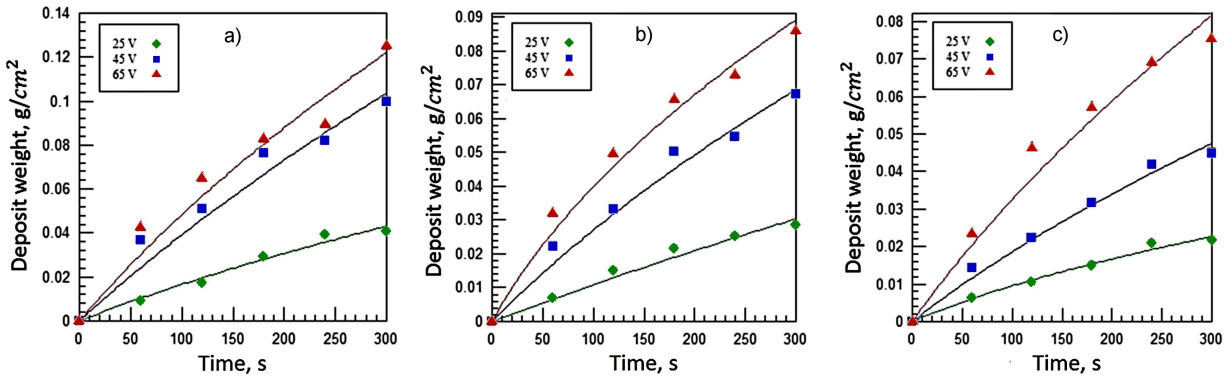

Figure 6. The variation in the deposit weight with time as well as fitting results of the experimental data to the model for different suspensions: a) YSZ-50 wt.% Al, b) YSZ-30 wt.% Al and c) YSZ

phenomenon causes aggregation of colloidal particles, which in turn can act as a barrier against movement of the particles towards an oppositely charged electrode, and consequently reduces the electrophoretic mobility of the charged particles [45,46]. Therefore, by comparing three coating compounds, the current density of suspension at a constant voltage has been enhanced by an increase of nanoparticles content in the suspension.

In order to completely characterize the EPD behaviour, deposit weight versus time measurements for different suspensions and at various constant voltages are conducted. Figures 6 and 7 show the non-linear correlation between deposit weight and time as confirmed by fitted curves.

The plots in Fig. 6 graphically present the effect of voltage on the deposit layer weight against time, as well as fitting of the experimental results to the curves of the Baldisserri model approached for different suspensions. The empirical results are consistent with the Baldisserri equation because the deposit weight has reached a constant value over time and the problem of formation of an insulating deposit layer has been accounted at longer times. Also, the driving force for the electrophoretic deposition is increased by increasing the voltage which is originated from Coulombic forces applied to the suspended particles within the suspension [24].

Figure 7 compares the variation in the weight of the deposition layer with time with respect to the change in the relative amount of materials in suspensions at various constant electric potentials. The variation of deposit weight obeys the Baldisserri equation. As it is seen in the figure, the rate of layer formation (curves slope) reduces by increasing time, and deposition yields decrease with the relative amount of the YSZ nanoparticles (decreasing micron-sized Al particles).

The experimental results of this study indicated that, despite the higher charge passed through suspensions containing more nanoparticles, the deposition weight decreased with increasing nanoparticles content. This can be attributed to an increase in the electrical conductivity of the suspension by adding nanoparticles. In fact, due to the high surface area of nanoparticles, the concentration of electrolyte in the suspension is increased and the zeta potential drops and consequently a lower rate coefficient k is expected for suspensions including more YSZ nanoparticles [29]. Moreover, a larger amount of free ions that may be formed in these suspensions will carry some electric charge, which in turn can lead to a decrease in the deposition rate of YSZ [34].

3.3. Effect of applied voltage on the coating microstructure

One major challenge of the EPD process is to achieve quality by preventing the formation of cracks due to the changes in temperature during drying and sintering of ceramic coatings. Because of the melting and oxidation

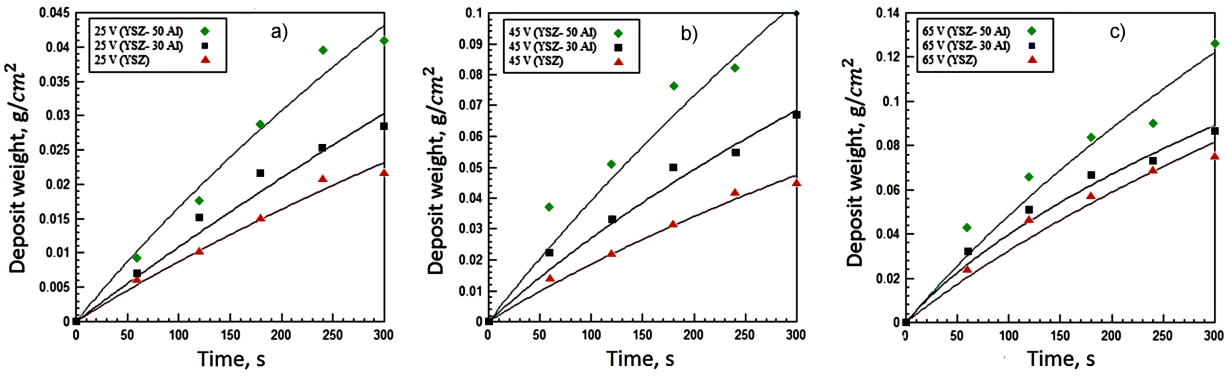

Figure 7. Effect of suspension composition on the curves of deposit weight versus time as well as fitting results for fixed applied fields: a) YSZ-50 wt.% Al, b) YSZ-30 wt.% Al and c) YSZ

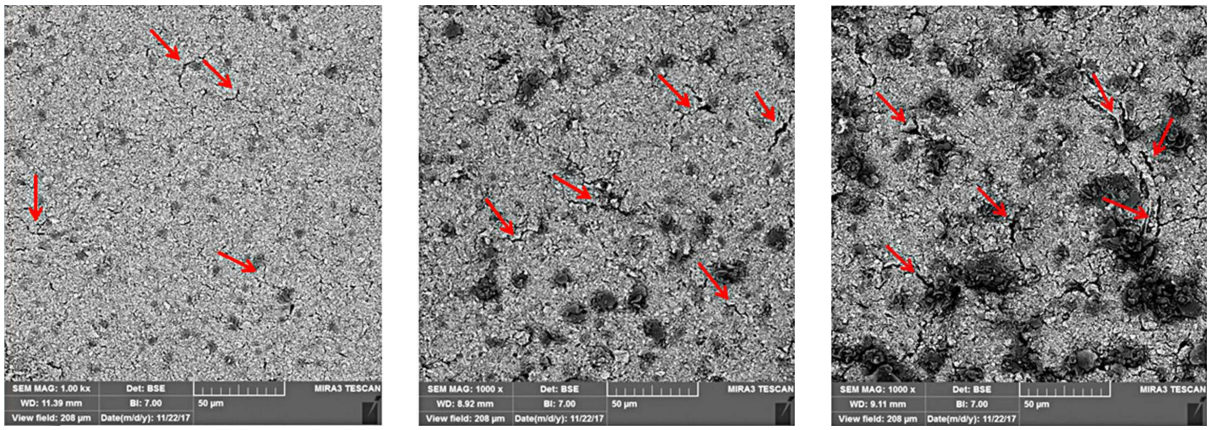

Figure 8. FE-SEM micrographs illustrating the morphology of the surfaces of YSZ/Al_2O_3 coating created by using YSZ-50 wt.% Al at different voltages for 1 min after sintering at 1150 °C: a) 25 V, b) 45 V and c) 65 V (cracks are indicated by red arrows)

of aluminium and subsequent *in situ* formation of alumina during the sintering of composite, the process of deposit compaction and bonding can be promoted at relatively low temperatures, which in turn can affect service reliability and mechanical integrity [31].

Figure 8 shows the FE-SEM micrographs from the surface of the sintered YSZ/Al_2O_3 coatings deposited from the suspension of YSZ-50 wt.% Al at different applied voltages (25, 45 and 65 V). As it is seen, increasing the applied voltage during EPD of this composite coating leads to the formation of cracked coatings after sintering at 1150 °C.

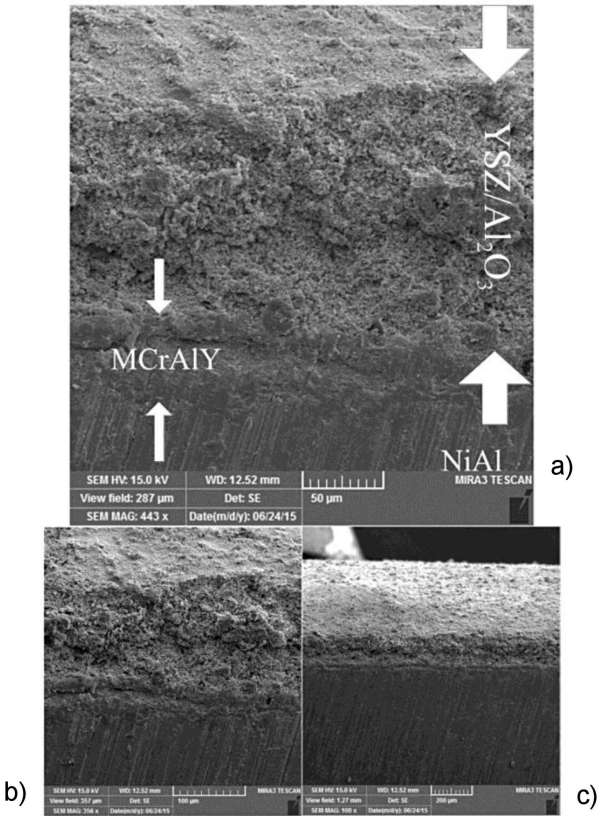

Figure 9. Cross-sectional views of YSZ/Al_2O_3 nanocomposite coating at different magnifications

According to the curves corresponding to the Baldisserri model, kinetic constants were greater at the higher voltages. Because of that the formation of particulate film on the substrate is a kinetically dependent phenomenon; the accumulation rate of the particles affects their packing behaviour and density of coatings. For a higher applied voltage, which may cause turbulence in the suspension, the deposit may be disturbed by flows in the surrounding media [2,47]. Another possible explanation for the formation of a porous, inhomogeneous microstructure is the higher deposition rate at a higher applied deposition voltage, so that the particles have no sufficient opportunity to move for rearrangement during deposition [48,49].

Ng and Boccaccini [35] proposed that when the applied field increases to a specified value, the rate of deposition can drop due to the interaction of deposited particles under very high driving forces. Consequently, a high level of non-uniformity develops and a porous coating forms [50]. This is in agreement with the change of EPD mechanism at higher voltages, as explained previously. This finding indicates that a uniform deposition can only be achieved within specified applied voltages [35]. At higher voltages, a dense structure is not created, and consequently cracks are made after sintering [2,49].

3.4. Cross-section of coated surface

Figure 9 shows the cross-sectional FE-SEM images of a typical coating prepared at voltage 45 V for 3 min and sintered at 1150 °C for 4 h. The micrographs confirm the formation of continuous ceramic coating onto the substrate without any cracks. However, it can be observed that the coating was bonded to the Inconel substrate via the MCrAlY intermediate layer. Inconel superalloys usually possess MCrAlY as an oxidation-resistant bond-coat (where M is Ni, Co, NiCo or CoNi depending on different working environments) [51].

As it can be seen from the FESEM micrograph presented in Fig. 9a, the thickness of the YSZ/Al_2O_3 nanocomposite coating is about 150 μm and that of the MCrAlY bond-coat layer is about 60 μm, which are in a

suitable range for TBC applications. Figures 9b and 9c represent low-magnification images of the coated surface. It can be found that the coating possesses a dense structure, crack-free morphology and it had a good adherence with the MCrAlY intermediate layer.

IV. Conclusions

The kinetics of the electrophoretic layer formation for suspensions containing different percent of yttria stabilized zirconia (YSZ) nanoparticles and micron-sized aluminium particles have been investigated at three different voltages. By plotting the current density-time curves and calculating time integrals of them, the passed charge versus time was determined for three suspensions (YSZ-50 wt.% Al, YSZ-30 wt.% Al and YSZ) at different voltages.

It was found that with the same initial particle concentration in the suspension, the current density and passed charge are higher when a higher voltage is applied. The kinetic aspects of EPD were demonstrated by the Baldisserri model through schematic plots of deposit weight against the passed charge or time. It was shown that the predictions of the utilized kinetic model (the Baldisserri model) agreed well with the experimental trend of deposit weight variations with time. Both calculation and measurement showed that by increasing time, voltage and amount of secondary phase in the composite, the mass of the deposits formed on the substrate increased. By increasing the voltage, the constants of the Baldisserri kinetic model were increased, whereas the rate coefficient k of the model was lower for the suspensions including more YSZ nanoparticles.

With increasing weight percent of the YSZ nanoparticles, the electrical conductivity and passed charges increased, but the rate of the layer formation decreased, possibly due to the presence of free ions. Aluminium particles have been found to improve deposition yields. At all voltages, in a short period of time, a linear relationship was observed between the amounts of the deposit weight with time, but it was removed from the linear state at longer times. Although when a higher voltage was applied, the deposition yields were higher, characterization of the coatings by FE-SEM indicated that the surface quality of coatings can suffer. By an increase in the applied voltage, the number of cracks made on the surface of the coating increased.

Acknowledgements: The authors would like to thank Islamic Azad University, Takestan Branch, for the financial support provided for the internal research work.

References

1. F. Guo, A. Javed, I.P. Shapiro, P. Xiao, "Effect of HCl concentration on the sintering behavior of 8 mol% Y_2O_3 stabilized ZrO_2 deposits produced by electrophoretic deposition (EPD)", *J. Eur. Ceram. Soc.*, **32** (2012) 211–218.
2. R.N. Basu, C.A. Randall, M.J. Mayo, "Fabrication of dense zirconia electrolyte films for tubular solid oxide fuel cells by electrophoretic deposition", *J. Am. Ceram. Soc.*, **84** (2001) 33–40.
3. K. Chen, Z. Lü, N. Ai, X. Huang, Y. Zhang, X. Xin, R. Zhu, W. Su, "Development of yttria-stabilized zirconia thin films via slurry spin coating for intermediate-to-low temperature solid oxide fuel cells", *J. Power Sources*, **160** (2006) 436–438.
4. M. Mori, Y. Itagaki, Y. Sadaoka, "VOC detection by potentiometric oxygen sensor based on YSZ and modified Pt electrodes", *Sensor. Actuat. B Chem.*, **161** (2012) 471–479.
5. E. Di Bartolomeo, M.L. Grilli, "YSZ-based electrochemical sensors: From materials preparation to testing in the exhausts of an engine bench test", *J. Eur. Ceram. Soc.*, **25** (2005) 2959–2964.
6. R. Moos, "A brief overview on automotive exhaust gas sensors based on electroceramics", *Int. J. Appl. Ceram. Technol.*, **2** (2005) 401–413.
7. X.Q. Cao, R. Vassen, D. Stoever, "Ceramic materials for thermal barrier coatings", *J. Eur. Ceram. Soc.*, **24** (2004) 1–10.
8. L.B. Chen, "Yttria-stabilized zirconia thermal barrier coatings - A review", *Surf. Rev. Lett.*, **13** (2006) 535–544.
9. M.P. Schmitt, A.K. Rai, R. Bhattacharya, D. Zhu, D.E. Wolfe, "Multilayer thermal barrier coating (TBC) architectures utilizing rare earth doped YSZ and rare earth pyrochlores", *Surf. Coat. Technol.*, **251** (2014) 56–63.
10. H. Maleki-Ghaleh, M. Rekabeslami, M.S. Shakeri, M.H. Siadati, M. Javidi, S.H. Talebian, H. Aghajani, "Nanostructured yttria-stabilized zirconia coating by electrophoretic deposition", *Appl. Surf. Sci.*, **280** (2013) 666–672.
11. O. Khanali, M. Rajabi, S. Baghshahi, S. Ariaee, "Suspension medium's impact on the EPD of nano-YSZ on Fecralloy", *Surf. Eng.*, **33** (2017) 310–318.
12. P. Wang, Y.D. He, S.D. Deng, J. Zhang, "Porous α-Al_2O_3 thermal barrier coatings with dispersed Pt particles prepared by cathode plasma electrolytic deposition", *Int. J. Miner. Metal. Mater.*, **23** (2016) 92–101.
13. C. Amaya, W. Aperador, J.C. Caicedo, F.J. Espinoza-Beltrán, J. Muñoz-Saldaña, G. Zambrano, P. Prieto, "Corrosion study of alumina/yttria-stabilized zirconia (Al_2O_3/YSZ) nanostructured thermal barrier coatings (TBC) exposed to high temperature treatment", *Corros. Sci.*, **51** (2009) 2994–2999.
14. S. Goel, S. Björklund, N. Curry, S. Govindarajan, U. Wiklund, C. Gaudiuso, S. Joshi, "Axial plasma spraying of mixed suspensions: A case study on processing, characteristics, and tribological behavior of Al_2O_3-YSZ coatings", *Appl. Sci.*, **10** (2020) 5140.
15. H. Huang, K. Eguchi, T. Yoshida, "Novel structured yttria-stabilized zirconia coatings fabricated by hybrid thermal plasma spraying", *Sci. Technol. Adv. Mater.*, **4** (2003) 617–622.
16. G. Soyez, J.A. Eastman, L.J. Thompson, G.-R. Bai, P.M. Baldo, A.W. McCormick, R.J. DiMelfi, A.A. Elmustafa, M.F. Tambwe, D.S. Stone, "Grain-size-dependent thermal conductivity of nanocrystalline yttria-stabilized zirconia films grown by metal-organic chemical vapor deposition", *Appl. Phys. Lett.*, **77** (2000) 1155–1157.
17. P. Sarkar, D. De, H. Rho, "Synthesis and microstructural manipulation of ceramics by electrophoretic deposition", *J. Mater. Sci.*, **39** (2004) 819–823.

18. C.T. Kwok, P.K. Wong, F.T. Cheng, H.C. Man, "Characterization and corrosion behavior of hydroxyapatite coatings on Ti6Al4V fabricated by electrophoretic deposition", *Appl. Surf. Sci.*, **255** (2009) 6736–6744.
19. Y. Sakka, T. Uchikoshi, "Forming and microstructure control of ceramics by electrophoretic deposition (EPD)", *KONA Powder Particle J.*, **28** (2010) 74–90.
20. E.-L. Zhang, K. Yang, "Coating of calcium phosphate on biometallic materials by electrophoretic deposition", *Trans. Nonferrous Met. Soc. China*, **15** (2005) 957–964.
21. L. Besra, M. Liu, "A review on fundamentals and applications of electrophoretic deposition (EPD)", *Prog. Mater. Sci.*, **52** (2007) 1–61.
22. P. Sarkar, P.S. Nicholson, "Electrophoretic deposition (EPD): Mechanisms, kinetics, and application to ceramics", *J. Am. Ceram. Soc.*, **79** (1996) 1987–2002.
23. S.-J. Ciou, K.-Z. Fung, K.-W. Chiang, "The mathematical expression for kinetics of electrophoretic deposition and the effects of applied voltage", *J. Power Sources*, **172** (2007) 358–362.
24. B. Ferrari, R. Moreno, "EPD kinetics: A review", *J. Eur. Ceram. Soc.*, **30** (2010) 1069–1078.
25. P. Collini, S. Kota, A.D. Dillon, M.W. Barsoum, A.T. Fafarman, "Electrophoretic deposition of two-dimensional titanium carbide (MXene) thick films", *J. Electrochem. Soc.*, **164** (2017) D573–D580.
26. M. Diba, D.W.H. Fam, A.R. Boccaccini, M.S.P. Shaffer, "Electrophoretic deposition of graphene-related materials: A review of the fundamentals", *Prog. Mater. Sci.*, **82** (2016) 83–117.
27. K. Verma, H. Cao, P. Mandapalli, R. Wille, "Modeling and simulation of electrophoretic deposition coatings", *J. Comput. Sci.*, **41** (2020) 101075.
28. C. Baldisserri, D. Gardini, C. Galassi, "An analysis of current transients during electrophoretic deposition (EPD) from colloidal TiO_2 suspensions", *J. Colloid Interf. Sci.*, **347** (2010) 102–111.
29. H. Farnoush, J. Aghazadeh Mohandesi, D. Haghshenas Fatmehsari, F. Moztarzadeh, "A kinetic study on the electrophoretic deposition of hydroxyapatite-titania nanocomposite based on a statistical approach", *Ceram. Int.*, **38** (2012) 6753–6767.
30. A.R.C. Sharman, J.I. Hughes, K. Ridgway, "Workpiece surface integrity and tool life issues when turning Inconel 718™ nickel based superalloy", *Mach. Sci. Technol.*, **8** (2004) 399–414.
31. O. Khanali, S. Baghshahi, M. Rajabi, "Fabrication and characterization of YSZ/Al_2O_3 nano-composite coatings on Inconel by electrophoretic deposition", *J. Mater. Res.*, **32** (2017) 3402–3408.
32. O. Khanali, S. Ariaee, M. Rajabi, S. Baghshahi, "An investigation on the properties of YSZ/Al_2O_3 nanocomposite coatings on Inconel by electrophoretic deposition", *J. Compos. Mater.*, **52** (2018) 81–89.
33. K. Maca, H. Hadraba, J. Cihlar, "Electrophoretic deposition of alumina and zirconia: I. Single-component systems", *Ceram. Int.*, **30** (2004) 843–851.
34. T. Ishihara, K. Shimose, T. Kudo, H. Nishiguchi, T. Akbay, Y. Takita, "Preparation of yttria-stabilized zirconia thin films on strontium-doped $LaMnO_3$ cathode substrates via electrophoretic deposition for solid oxide fuel cells", *J. Am. Ceram. Soc.*, **83** (2000) 1921–1927.
35. S.Y. Ng, A.R. Boccaccini, "Lead zirconate titanate films on metallic substrates by electrophoretic deposition", *Mater. Sci. Eng. B*, **116** (2005) 208–214.
36. V. Tizjang, M. Montazeri-Pour, M. Rajabi, M. Kari, S. Moghadas, "Surface modification of sol-gel synthesized TiO_2 photo-catalysts for the production of core/shell structured TiO_2-SiO_2 nano-composites with reduced photocatalytic activity", *J. Mater. Sci. Mater. Electron.*, **26** (2015) 3008–3019.
37. S. Cabanas-Polo, A.R. Boccaccini, "Electrophoretic deposition of nanoscale TiO_2: Technology and applications", *J. Eur. Ceram. Soc.*, **36** (2016) 265–283.
38. A. Szydło, J.-D. Goossen, C. Linte, H. Uphoff, M. Bredol, "Preparation of platinum-based electrocatalytic layers from catalyst dispersions with adjusted colloidal stability via a pulsed electrophoretic deposition method", *Mater. Chem. Phys.*, **242** (2020) 122532.
39. D. Das, B. Bagchi, R.N. Basu, "Nanostructured zirconia thin film fabricated by electrophoretic deposition technique", *J. Alloys Compd.*, **693** (2017) 1220–1230.
40. M.J. Santillán, F. Membrives, N. Quaranta, A.R. Boccaccini, "Characterization of TiO_2 nanoparticle suspensions for electrophoretic deposition", *J. Nanoparticle Res.*, **10** (2008) 787–793.
41. P.S. Nicholson, P. Sarkar, X. Haung, "Electrophoretic deposition and its use to synthesize ZrO_2/Al_2O_3 microlaminate ceramic/ceramic composites", *J. Mater. Sci.*, **28** (1993) 6274–6278.
42. A.G. Bhosale, M.B. Kadam, R. Joshi, S.S. Pawar, S.H. Pawar, "Studies on electrophoretic deposition of nanocrystalline SDC electrolyte films", *J. Alloys Compd.*, **484** (2009) 795–800.
43. M. Montazeri-Pour, M.H. Parsa, "Constitutive analysis of tensile deformation behavior for AA1100 aluminum subjected to multi-axial incremental forging and shearing", *Mechan. Mater.*, **94** (2016) 117–131.
44. B. Ferrari, R. Moreno, "The conductivity of aqueous Al_2O_3 slips for electrophoretic deposition", *Mater. Lett.*, **28** (1996) 353–355.
45. R. Rojaee, M. Fathi, K. Raeissi, "Electrophoretic deposition of nanostructured hydroxyapatite coating on AZ91 magnesium alloy implants with different surface treatments", *Appl. Surf. Sci.*, **285** (2013) 664–673.
46. J. Ma, C. Wang, K.W. Peng, "Electrophoretic deposition of porous hydroxyapatite scaffold", *Biomaterials*, **24** (2003) 3505–3510.
47. M. Jafarpour, H. Aghajani, "Electrophoretic deposition of bi-layered nano-sized silicon carbide/mullite coating from stabilized suspensions", *J. Aust. Ceram. Soc.*, **56** (2020) 761–770.
48. J. Ma, W. Cheng, "Electrophoretic deposition of lead zirconate titanate ceramics", *J. Am. Ceram. Soc.*, **85** (2002) 1735–1737.
49. A. Araghi, M.J. Hadianfard, "Fabrication and characterization of functionally graded hydroxyapatite/TiO_2 multilayer coating on Ti-6Al-4V titanium alloy for biomedical applications", *Ceram. Int.*, **41** (2015) 12668–12679.
50. J. Chen, H. Fan, X. Chen, P. Fang, C. Yang, S. Qiu, "Fabrication of pyrochlore-free PMN-PT thick films by electrophoretic deposition", *J. Alloys Compd.*, **471** (2009) L51–L53.
51. M. Bai, F. Guo, P. Xiao, "Fabrication of thick YSZ thermal barrier coatings using electrophoretic deposition", *Ceram. Int.*, **40** (2014) 16611–16616.